Energy Loss from Reconnection with a Vortex Mesh

I.H. Neumann and R.J. Zieve
Physics Department, UC Davis

Experiments in superfluid ^{4}He show that at low temperatures, energy dissipation from moving vortices is many orders of magnitude larger than expected from mutual friction. Here we investigate other mechanisms for energy loss by a computational study of a vortex that moves through and reconnects with a mesh of small vortices pinned to the container wall. We find that such reconnections enhance energy loss from the moving vortex by a factor of up to 100 beyond that with no mesh. The enhancement occurs through two different mechanisms, both involving the Kelvin oscillations generated along the vortex by the reconnections. At relatively high temperatures the Kelvin waves increase the vortex motion, leading to more energy loss through mutual friction. As the temperature decreases, the vortex oscillations generate additional reconnection events between the moving vortex and the wall, which decrease the energy of the moving vortex by transfering portions of its length to the pinned mesh on the wall.

Introduction

Energy transfer in superfluids is closely tied to the quantized vortex lines present in any non-trivial flow [1]. In a superfluid the curl of the velocity field vanishes except along isolated vortex cores, and its values along the cores lead to quantized circulation within the superfluid. Superflow, with no energy loss, occurs only at sufficiently low speeds. Higher velocities lead to creation of vortices, which extracts energy from the flow, and then to further energy loss as those vortices move.

Early measurements of energy dissipation in superfluid ^{4}He include second-sound propagation through vortex arrays in uniformly rotating resonators [2] and electrical detection of individual charged vortex rings moving through an otherwise stationary fluid [3]. These experiments show that dissipation depends strongly on the fluid's temperature as well as on the vortex velocity. At relatively high temperatures, above 1 K, thermal excitations behave like a normal liquid of density ρ_n, coexisting with a superfluid of density ρ_s. The sum $\rho_n + \rho_s$ gives the total fluid density. Since a vortex core is an excitation but the flow about the core is superfluid, vortices couple the two fluids through a force known as mutual friction. Experimentally, the mutual friction force per unit length of vortex is [4]

$$\mathbf{F}_f = \alpha\kappa\rho_s(\mathbf{v}_n - \mathbf{v}_L). \quad (1)$$

Here κ is the circulation around the moving vortex, α is an experimentally determined friction parameter, and $\mathbf{v}_n$ and $\mathbf{v}_L$ are the velocities of the normal fluid and the vortex, respectively. In general the mutual friction force has an additional component perpendicular to the vortex line's velocity, which we neglect because its magnitude is much smaller [2].

Well below 1 K, the normal fluid fraction becomes negligible and transfer of energy from the superfluid to normal component through mutual friction is no longer significant. Recent interest in low-temperature dissipation mechanisms has centered around the problem of superfluid turbulence, where groups of vortices form tangles which highly resemble classical turbulence. Many length scales are represented in the tangles, depending on the curvatures of different vortex segments, and the velocity field changes drastically on short length scales near any individual vortex core. Above 1 K, turbulence generated on a macroscopic length scale, as by rotating blades [5], a towed grid [6], or spin-down of a rotating container [7], shows the same energy spectrum and time decay as turbulence in classical fluids. This can be explained as classical turbulence in the normal component, coupled to the superfluid through mutual friction. As temperature decreases, the decay rate for vortex line length drops abruptly near 0.8 K [7], although the functional form remains unchanged. This indicates a change in the mechanisms for dissipating energy or for transfering energy to smaller length scales. When the turbulence is created directly by injecting microscopic vortex rings, the functional form itself changes at low temperatures [8, 9]. A similar effect is seen with inhomogeneous tangles in superfluid ^{3}He-B [10]. Current ideas for the low-temperature dissipation mechanism center on vortex reconnections and on phonon emission by Kelvin waves along vortex lines [11, 12]. To explore such ideas, further experiments and simulations are needed.

Our present work is motivated by measurements in a unique single-vortex geometry [13]. A fine wire, stretched along the axis of a cylinder filled with superfluid, traps a vortex. If the vortex partially depins from the wire and continues from the wire to the curved cell wall, as illustrated in Figure 1, the free portion of the vortex moves through the cell at the local superfluid velocity. Since the velocity field is determined primarily from the location of the vortex core, the free end precesses about the wire. During the precession, the portion of the vortex that remains trapped about the wire decreases in length, which indicates that the moving vortex dissipates energy. However, the mechanism is unclear; at the lowest temperatures, near 320 mK, the dissipation is many orders of magnitude larger than could occur through mutual friction. We note that the vortex velocity in this measurement is very slow, roughly 0.003 cm/s as opposed to 20-120 cm/s in [3]. Other measurements do find some velocity dependence in the mutual friction coefficient α at high temperature, but this effect is negligible below 1 K [14]. Furthermore, the rate of energy loss through mutual friction should be proportional to α, but in fact the measured energy loss has far less temperature dependence than α. This suggests that a different mechanism is at work.

The likely source of the observed dissipation is a vortex-

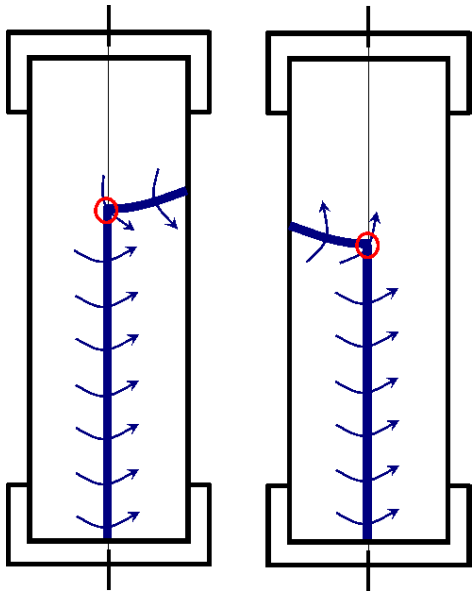

FIG. 1: A vortex partially pinned to a wire, with core in blue, at two different times. The point where the vortex detaches from the wire is marked with a red circle. The unpinned portion precesses about the cylindrical cell. Arrows represent the velocity field near the vortex core.

wall interaction. Since the moving vortex terminates on the container wall, it can interact with the surface in addition to undergoing vortex-fluid interactions along its length. The exact mechanism of the vortex-wall interaction is unknown. Possibilities suggested previously include viscous drag through a normal-fluid Ekman layer near the surface and a force from vortex line tension [15]. Since neither of these completely fits the experimental results [16], we here investigate another possibility: an interaction with microscopic vortex segments pinned to the cell wall. As the moving vortex line sweeps along the wall, it encounters pinned vortices. Closely approaching vortices undergo reconnections, and the moving vortex may gradually shrink if it leaves pieces of itself behind on the cell wall. In this paper we describe numerical simulations of the process. In common with the recent efforts on superfluid turbulence, it proves to depend heavily on interplay between vortex reconnections and the Kelvin waves they generate.

Computational Model

We follow the method originally used by Schwarz for modeling vortex dynamics [17]. As described elsewhere [18–22], we treat the vortex cores as massless and thin; that is, the core diameter is small compared to the curvature along the core. The equation governing the motion of superfluid vortices is essentially the Euler equation for incompressible fluid flow, with an additional term for mutual friction between the vortices and normal fluid. Physically, in the absence of friction, the vortex cores move at the local superfluid velocity. In our code, we specify a vortex by a series of points along its core and update each point based on the fluid velocity at that location, calculated in the local induction approximation. Details of our algorithm appear in [23]. We use a fourth-order Runge-Kutta-Felberg (RKF) method with a variable time step for solving the ordinary differential equation. We determine the step size by requiring third-order and fourth-order RKF calculations to agree to 0.1%.

We calculate the superfluid velocity field from the positions of the vortex cores, adding an additional zero-curl field to ensure that the boundary condition at the wall is satisfied: namely, that the velocity component perpendicular to the wall must vanish at the wall. In the present work we compute this boundary field approximately using image vortices, as described below.

Following [17], we include a mutual friction term based on Equation 1. The friction term damps out oscillations of the vortex lines, keeping the simulations stable. For this purpose we use values of α from 0.001 to 0.1, which are much larger than the actual friction coefficient $\alpha = 5 \times 10^{-10}$ for superfluid helium at our experimental temperature [24]. The temperatures corresponding to the friction coefficients in our simulations are 850 mK to 1.6 K.

In the present simulations, we omit an explicit calculation of the contributions to the velocity field from distant vortex cores. Instead we incorporate their influence through reconnections. The velocity field due to a vortex falls off quickly with distance, so it is reasonable to consider only close neighbors. Furthermore, there is some averaging of the contributions from more distant vortices. Reconnections occur because, for most vortex orientations, two closely approaching vortices attract each other with increasing strength [17, 25]. They form cusps, which get drawn out ever larger. Simulations typically break down in this regime, on account of the rapidly varying velocity fields that nearby vortices feel from each other. Experiments show reconnections of the two vortices, with the new formations then moving apart from each other [26]. Following [17], we reconnect any two vortices that approach each other closer than a cutoff distance. To avoid recurring reconnections between the same pair of vortices, a vortex segment that has just undergone a reconnection cannot reconnect again for a brief period. This allows the newly reconnected segments to separate beyond the reconnection distance.

We also allow reconnections between a vortex and the cell wall. Since the effect of a surface can be treated with image vortices, a vortex which closely approaches the wall undergoes a cusp formation similar to that in vortex-vortex interactions. When the vortex touches the wall, two new vortex endpoints form and proceed to move apart from each other.

We simulate the motion of a vortex that runs from the cylinder axis to its curved wall. We assume that the end that reaches the axis continues as a straight, stationary vortex along the axis, analogous to the experimental situation described above with a vortex line partially pinned to a central wire [13]. In addition, we consider a mesh of microscopic vortices attached to the surface of the cell. Because of the extremely small coherence length in superfluid ^{4}He, such pinned vortices ap-

pear upon cooling through the superfluid transition temperature, where the energy barrier to vortex creation is small [27]. They can also appear when the cryostat rotates, as it does in the experiment. Rotating creates an array of straight vortex lines parallel to the rotation axis. Once rotation ceases, these vortices annihilate at the cell wall, which is rough on the scale of a superfluid vortex. Fragments of the vortices could remain pinned between small protrusions along the cell's walls, as illustrated in Figure 2. We examine how such a mesh of microscopic vortices affects the macroscopic vortex running from the wire to the cell wall.

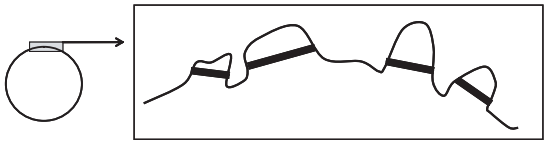

FIG. 2: An exaggerated schematic of the cylinder wall's roughness. Mesh vortices pin to protrusions and are pulled taut between them.

We do not attempt to model the cell's surface roughness explicitly; instead we define certain points on the cylinder's wall as the endpoints of pinned vortices. From previous work, we know that the only stable macroscopic vortices pinned at both ends to the cylinder wall have significant horizontal components and span much of the cell [23]. However, the mesh we envision here consists of much shorter vortices. On their length scale the wall does not resemble a smooth cylindrical surface and the earlier calculation does not apply. For most of our work here, we assume that the mesh vortices are stretched taut between their two endpoints. Figure 2 shows our picture of vortices pinned to the wall. Alternatively, in a few calculations we use semicircular rather than straight-line vortices. In generating the pinned vortices, we can vary their number, length, and orientation.

To set up the initial vortex mesh, we select a portion of the cell wall on which the vortices can lie. We then choose a random point within this region as one end of a mesh vortex. We choose the second endpoint relative to the first one. The orientation and length of the vortex each can be fixed or can be chosen at random within a selected range. We then repeat the process to generate a target number of mesh vortices. One final step is needed for simulations with random orientations. Our algorithm requires only the first endpoint to lie within the selected region, so all vortices that cross the edge of the mesh region initially point outwards. We eliminate this bias by flipping the orientation of each vortex with 50% probability.

Our RKF algorithm updates only the position of the vortex line which stretches from the cylinder axis to the wall. The mesh vortices and the vortex portion running along the cylinder axis remain stationary.

As noted above, we use image vortices to satisfy the boundary conditions for the velocity field approximately. For the central vortex, we extend it along the cylinder axis to negative infinity, and also continue the other end from the curved wall to infinity as a straight, radial vortex. For the mesh vortices, we note that at an infinite plane boundary, image vortices produce an exact solution to Laplace's equation that satisfies the boundary condition. Since the mesh vortices are extremely short compared to the cylinder radius, the cylinder wall can be treated as nearly flat, apart from the wall roughness. To adjust for its curvature, we invert each mesh vortex in the cylinder, so that with its image it becomes a vortex ring. To the extent that these methods do not perfectly meet the boundary conditions, we can picture deformations in the cylinder which do make its surface perpendicular to the velocity field. These deformations are a type of wall roughness, which we already assume exists when we define the vortex mesh.

As the moving vortex sweeps along the wall, it encounters mesh vortices and undergoes reconnections. In principle, the moving vortex could also bend enough that it reconnects with itself, but in practice this does not happen for the present geometry. When a reconnection occurs, one endpoint of the mesh vortex becomes the wall terminus of the moving vortex while the original wall terminus becomes a mesh vortex endpoint. We then redefine the mesh vortex using the new endpoints and assuming it runs directly between them. Straightening the mesh vortex makes sense because the actual motion after a reconnection involves oscillations stemming from cusp formation at the reconnection point [17, 25, 26]. The vortex gradually loses energy through these oscillations, and a pinned vortex would eventually become straight. Although we do not calculate the oscillations of the pinned vortex after each reconnection, in the corresponding experiment the pinned vortices do have plenty of time to settle before the moving vortex interacts with them, so they are likely to be nearly straight.

More detailed simulations [28] show that vortex reconnections release energy into sound waves. However, the energy loss is so small that thousands of reconnections per second would be required to match our experimental observations. The present work investigates less direct energy consequences of reconnections. Our reconnection algorithm identifies the points of closest approach of two vortices, then moves out along each vortex a distance comparable to the vortex separation. We delete the segments near the reconnection points and replace them with segments crossing between the original vortices, as shown in Figure 3. With the numbers we use for the various lengths, on average the vortex length actually increases slightly through reconnections. Thus we are not trivially introducing energy loss to our simulation through the numerics of our reconnections.

In our previous calculations on nearly stationary vortices, we subtracted the velocity tangent to the vortex core before updating the configuration. Here we keep the tangential component. Points along the vortex line occasionally bunch up or separate too far, so we delete or add points as appropriate to keep neighboring point spacings fairly uniform. Near the cell wall the point spacing must be smaller than the length of the mesh vortices. However, maintaining such a small spacing along the entire moving vortex would require vast numbers of data points, with correspondingly long computation times. Since the moving vortex has a much larger radius of curvature once it leaves the wall region, a lower density of points is adequate. We increase the point spacing by an order of magnitude far from the cell wall.

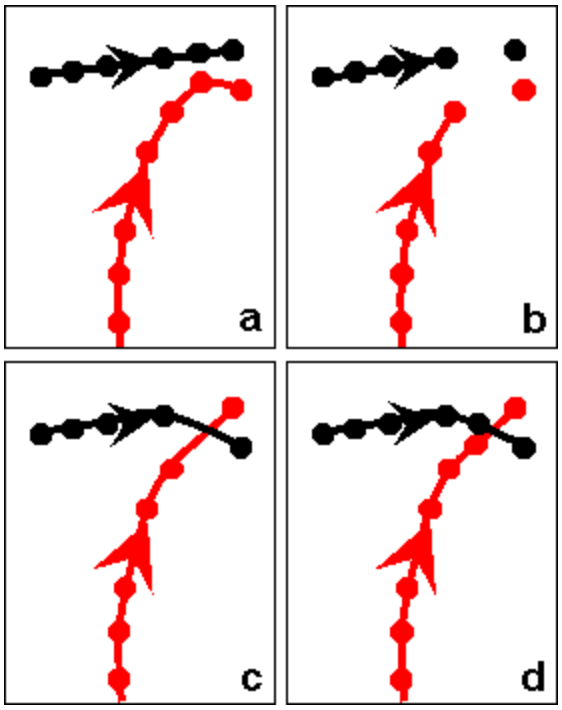

FIG. 3: Reconnection between two vortices. Vortices approach each other (a). At least one point on each vortex is removed (b). Remaining points on either side of the removed point are reconnected, swapping between vortices (c). If the new straight segments are too long, additional points are inserted (d).

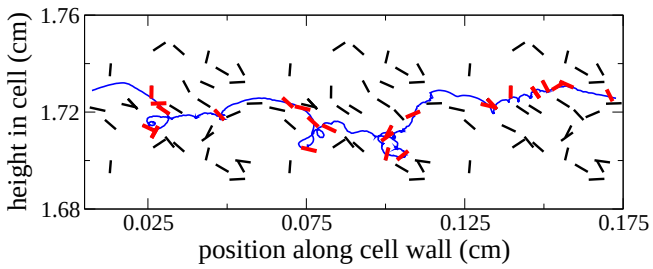

FIG. 4: During one run with $\alpha = 0.01$, the wall terminus of the moving vortex follows the path along the cylinder wall indicated by the long blue curving trace. The mesh vortices it reconnects with are thick and red, while the other mesh vortices are thinner and black.

Any reconnection produces oscillations along the new vortex lines [29, 30]. Immediately after a reconnection sharp kinks in the moving vortex appear close to the wall. As the vortex line tension acts on the kinked regions, characteristic Kelvin oscillations ensue. Mutual friction damps out the Kelvin oscillations from a single reconnection, but a steady rate of reconnections can maintain the oscillatory motion. The oscillations persist along the entire vortex, with most of the additional motion vertical. For our moving vortex, the oscillations increase the distance the vortex travels over the cell wall, enabling it to encounter additional mesh vortices and undergo further reconnections. Figure 4 illustrates the path of the vortex endpoint and the wall vortices it encounters along the way.

Due to limits in computational power, populating the entire wall of the cell with mesh vortices is not feasible. Rather, we define mesh vortices over a portion of the cell wall near the wall terminus of the moving vortex line. The mesh region is an order of magnitude larger than the distances at which reconnections take place, so pinned vortices outside the region would at first have no effect under our algorithm. However, as the macroscopic vortex precesses, it can leave the initially defined region. To mimic vortices covering the entire cell wall, the mesh region must move to track the precessing vortex. If both endpoints of a mesh vortex are at least 30% of the mesh width behind the moving vortex in the angular direction, we translate that vortex by exactly the angular width of the mesh to a new position ahead of the moving vortex. Conversely, if a mesh vortex is at least 70% of the mesh width ahead of the moving vortex, we translate that mesh vortex back to a new position behind the moving vortex. The asymmetric conditions adjust for the prevailing motion of the partially trapped vortex. Similarly, a vortex that lies above (below) the moving vortex by at least half the mesh height is translated downward (upward) by the mesh height. Here the symmetric conditions reflect that the predominant vertical motion comes from oscillations. Figure 5 illustrates moving the mesh in the angular direction. The region of vortices marked in red on the right of the patch are shifted to the left of the patch at a later time. In this manner the moving vortex continues to encounter mesh vortices, but we limit our calculations to the relevant portions of the cell. We update the mesh position every 2000 to 6000 time steps, during which the vortex never traverses more than 30% of the mesh region.

Each simulation begins with 40 to 200 mesh vortices. We create no new mesh vortices during a simulation, but we remove vortices if their length falls below a minimum value. Hence the number of pinned vortices gradually decreases as the reconnections proceed, and the mesh eventually vanishes. One problem that sometimes arises is that the mesh develops a gap around the moving vortex, as shown in Figure 6. This typically happens when the mesh patch covers an insufficient width along the cell wall. Because of the way we translate the mesh to keep it centered about the moving vortex, a vortex that sweeps too fast horizontally relative to its vertical motion can pass through a given horizontal portion of the mesh multiple times before ever encountering other portions. If a gap appears during a run, we discard that run and repeat with a mesh that extends farther horizontally.

Results and Discussion

We find that a vortex mesh can enhance the energy dissipation of a moving vortex beyond what it would be with no mesh present. Figure 7 shows the vertical position of one end of the moving vortex, where it reaches the cylinder axis. The oscillations are generated by reconnections at the opposite end of the free vortex. They continue along the entire vortex line, with amplitude determined by the friction coefficient α. The dashed red line for the first 1200 seconds and the solid yellow

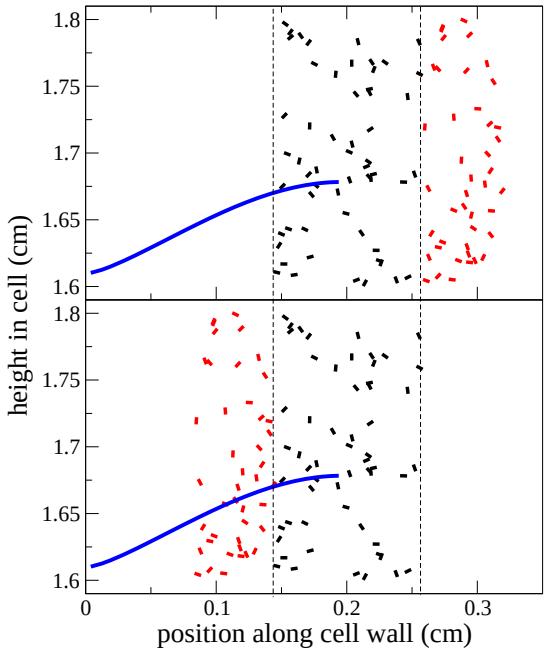

FIG. 5: Before moving a mesh patch (top) and after moving the mesh patch (bottom). The long, moving vortex is on the left in blue. The patch of mesh that moves, colored red, is to the right of the second vertical dotted line before moving and left of the first vertical dotted line after moving. The black vortices between the two vertical dotted lines do not move in this step.

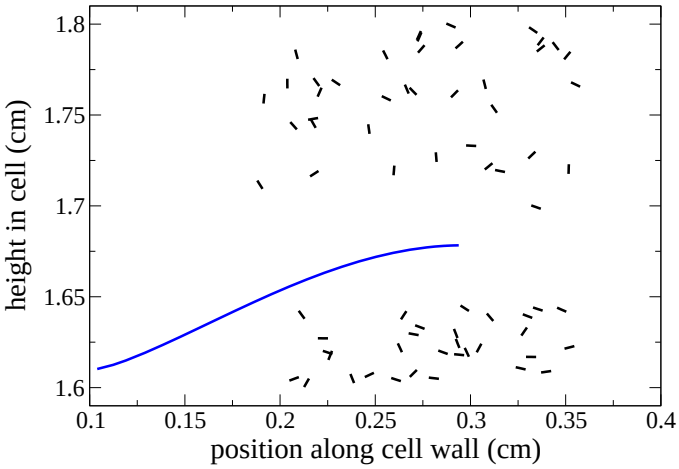

FIG. 6: Example of a run where a gap has opened in the mesh. The moving vortex is the long solid blue curve extending from the left into the mesh patch.

line for subsequent times indicate the average height of the vortex detachment point. Its decreasing value indicates that the vertical portion of the vortex shrinks. Since the portion of the vortex trapped around the wire is isolated and straight, its kinetic energy is proportional to its length and the motion of the detachment point indicates energy loss from the trapped vortex. The long-time behavior in this run gives a baseline for dissipation in the absence of mesh vortices. In the initial portion of the simulation, where the mesh is present, the energy loss is markedly higher. As seen from the inset, the mesh disappears shortly before 1600 seconds, coinciding with the change in the rate of energy loss.

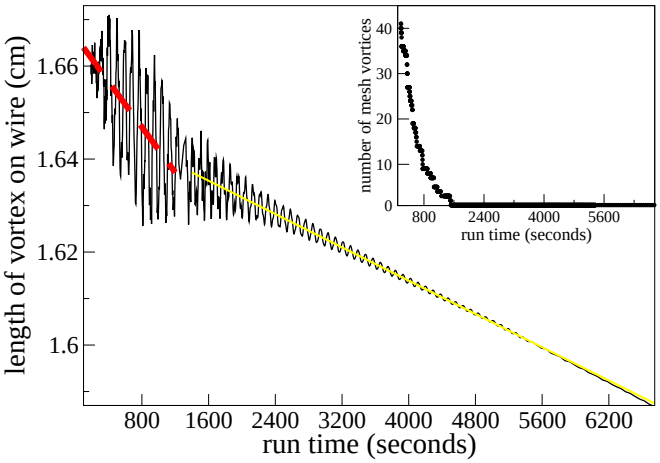

FIG. 7: Vertical position of the end of the moving vortex on the cylinder axis, for a run with α = 0.01. During the first 1000 seconds the vortex interacts with a mesh on the wall. The thick red dashed line indicates the average position during this time. At later times, the thick yellow solid line gives the average location. Inset: number of mesh vortices remaining as a function of time.

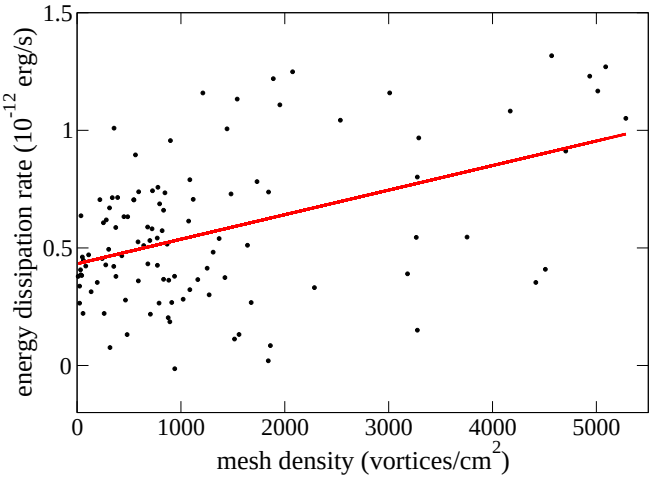

FIG. 8: Each circle gives average energy loss and average density for a segment of a run. See text for further explanation. The red line is a best fit to these points. Its positive slope shows increase of the moving vortex's energy dissipation with mesh density. The data shown here come from 18 independent runs each using α = 0.01 and beginning with randomly oriented mesh vortices of length 0.008 cm.

To show more clearly the role of the mesh, we calculate energy dissipation from the trapped vortex as a function of the number density of mesh vortices. Time traces, such as that in Figure 7, are divided into segments 100 to 300 seconds long,

so that the density is close to constant. For each segment we calculate the average values of quantities including number density, energy loss, length of the moving vortex, and total length of the mesh vortices. For $\alpha = 0.1$ and $\alpha = 0.01$, the time constants for decay for the lowest-frequency Kelvin oscillations are 120 s and 1200 s, respectively, with the faster oscillations that contribute most to energy dissipation decaying even more rapidly. As a result the behavior during different time segments is relatively independent. For $\alpha = 0.001$, with a time constant of 12,000 s for the slowest mode, we instead use only a single time segment near the beginning of each run, defined by when the number of mesh vortices is between 90% and 70% of the original number. We select only one segment because the extremely long time constant means that behavior late in a run depends not only on the instantaneous mesh density but also on the mesh present earlier in the run. We combine data from runs with the same friction parameter, mesh vortex length, and distribution of initial vortex orientations. Figure 8 shows how the energy dissipation rate depends on mesh density, with each point corresponding to one segment. The dissipation does increase with density, supporting the idea that reconnections contribute to the energy loss.

Why reconnections increase energy loss from the moving vortex is not obvious. One possibility is that the reconnections, on average, transfer pieces of the moving vortex to the wall. Yet although the length of the moving vortex can decrease during a reconnection, it can also increase. During a reconnection the moving vortex loses the portion between where it intersects the trapped vortex and the wall. On the other hand, it adds the portion from one end of the mesh vortex to the intersection point, as well as adding energy because the reconnection generally results in high local curvature. Most of our simulations use straight mesh vortices pulled taut between two pin sites, minimizing the additional length added to the moving vortex. Changing the shape of the mesh vortices does have a significant effect. We did a few calculations with semicircular mesh vortices, where the curvature leads to a longer mesh vortex length between the reconnection site and the wall. With semicircular vortices, the moving vortex *gains* energy through reconnections. For the physical experiment, straight vortices seem more plausible. A pinned vortex can dissipate energy through oscillations until it arrives at its lowest-energy configuration, which will usually be close to straight. If the vortex has too much curvature, it will encounter the wall during its oscillations and either annihilate or break into smaller, straighter vortices.

By monitoring the length of the moving vortex immediately before and after a reconnection, we find that even for straight wall vortices, vortex-vortex reconnections in our simple reconnection scheme usually lengthen the moving vortex. Thus these reconnections do not directly reduce the energy of the central vortex. Rather, the energy loss in our simulations comes from two other sources. Reconnections between the moving vortex and the cell wall *always* shorten the vortex since a piece remains behind, attached to the wall. In addition, the Kelvin waves generated by reconnections lead to an increase in the dissipation from mutual friction. We find that the former mechanism dominates at low α, the latter at high α.

friction coefficient α	energy loss no mesh present (10^{-12} erg/s)	energy loss dependence on mesh density (10^{-10} erg/s per vortex/cm^2)
0.1	4.35	0.717
0.01	.477	0.595
0.001	.0472	2.62

TABLE I: Comparison of energy loss with and without reconnections, for several values of friction coefficient. The values in the second and third columns are the y-intercepts and slopes, respectively, of the best-fit lines in Figure 9.

The change in mechanism is reflected in Figure 9, which shows energy dissipation rates as a function of mesh density for the three friction coefficients. All initial mesh vortices have length 0.008 cm and random orientations. In each case the dissipation rate increases with mesh density. However, the relative influence of the mesh is greater for smaller α. At high enough mesh density even the absolute effect of the mesh is larger for small α; the dissipation for $\alpha = 0.001$ actually *exceeds* that for $\alpha = 0.01$. These results for different friction coefficients are summarized in Table I; without a mesh the energy loss comes entirely from mutual friction and scales with α, but the mesh has more influence as α decreases.

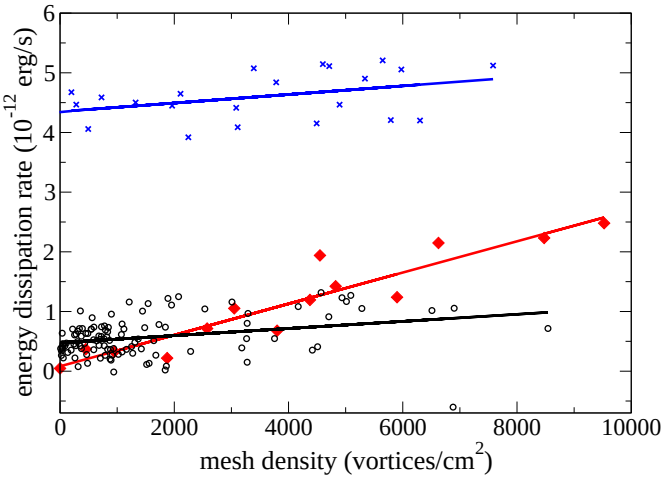

FIG. 9: Energy dissipation as a function of mesh density, for different friction coefficients. Red filled diamonds: α = 0.001; black open circles: α = 0.01; blue X's: α = 0.1. Lines are best fits to each data set. The mesh has a much stronger effect at the lowest friction, and at high mesh density the dissipation at $\alpha = 0.001$ actually exceeds that at $\alpha = 0.01$.

At the higher values of α, the pattern of reconnections is typically a vortex-vortex event followed not long after by a vortex-wall event. The first reconnection of a run is always vortex-vortex, and we never observe consecutive vortex-wall reconnections. Thus the wall reconnections occur only because the Kelvin oscillations resulting from the original reconnection bring another piece of the long vortex into prox-

imity with the wall. The single vortex-wall event provides no direct explanation for why the mesh increases energy loss; on average the combination of a vortex-vortex and ensuing vortex-wall reconnection gives a slight increase in the moving vortex length. However, the Kelvin waves produced along the vortex drastically increase its velocity. Since dissipation from mutual friction depends on the square of velocity, this has a major effect on the energy loss. For straight wall vortices, it more than compensates for the slight length increase due to reconnections.

For $\alpha = 0.001$, corresponding to a temperature of 850 mK in superfluid helium, the loss to mutual friction is small even with the induced oscillations. The low mutual friction means that the Kelvin waves along the vortex persist for long times, which permits a different form of energy loss. Each vortex-vortex reconnection leads to a series of vortex-wall reconnections, often 100 or more. As at higher α, the vortex mesh initiates this process; the first reconnection again is *always* with another vortex. If vortex-wall reconnections outnumber vortex-vortex events even slightly, the net effect is shortening of the moving vortex; with the large number of wall events at $\alpha = 0.001$, the energy loss from the central vortex is substantial. As Figure 9 shows, this mechanism which relies on low bulk mutual friction can produce larger energy loss than exists at higher α.

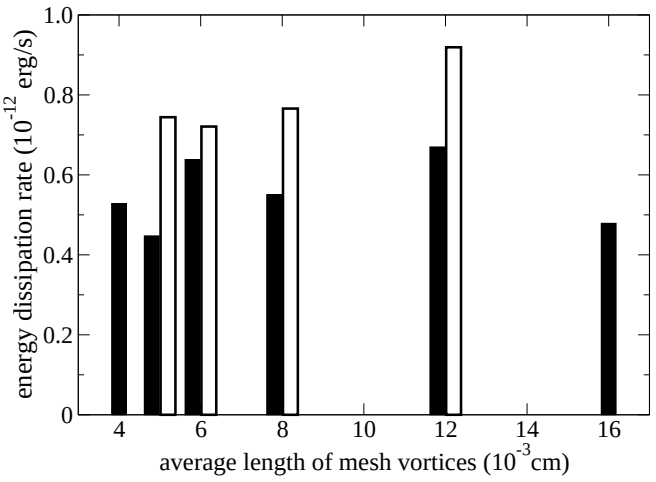

FIG. 10: Dissipation for simulations with varying mesh vortex lengths. Greater dissipation is seen in the heterogeneous length mixtures shown as unshaded columns. Runs with homogenous mesh vortex lengths are shown in black.

Other features that the mesh would have in a physical experiment appear to enhance the energy loss. Figure 10 shows how energy loss depends on the lengths of individual mesh vortices. When the mesh is homogeneous, consisting entirely of vortices of a single length, the energy loss is independent of the vortex length. Only the number density of vortices matters, as is natural if reconnections lead to energy loss mainly through the Kelvin waves they engender. As the mesh vortices get longer, the typical length added to the moving vortex during a reconnection also increases. However, this additional length is immediately removed during the subsequent vortex-wall reconnection.

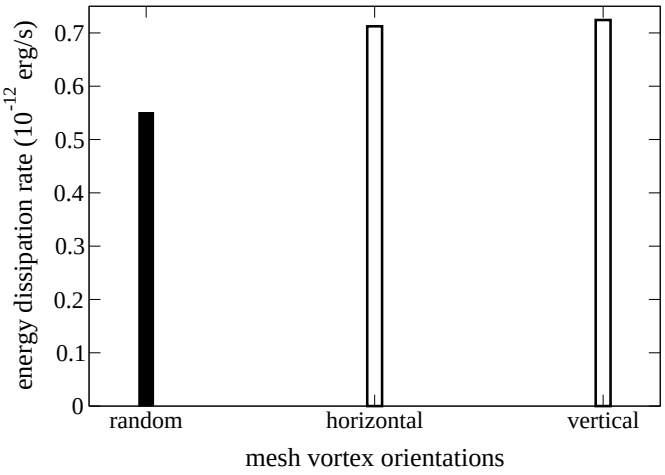

FIG. 11: Plot of dissipation for simulations with varying mesh vortex orientations. Greater dissipation is seen the predominantly horizontal ($\pm 22.5^\circ$) and vertical ($\pm 45^\circ$) textures (shown as empty columns) than in the one with random orientations (black column). All data have α = 0.01 and mesh vortex lengths of 0.008 cm.

Heterogeneous mixtures of vortex lengths behave differently. We use flat distributions of vortex length in ranges from 0.004 to 0.006 cm, 0.004 to 0.008 cm, 0.004 to 0.012 cm, and 0.008 to 0.016 cm. On comparing runs with a heterogeneous mesh to those with a homogeneous mesh of the same average vortex length, we consistently find a higher energy dissipation rate for the heterogeneous case. Reconnections occur at a faster rate for the heterogeneous mesh, with relatively little length gain but fewer vortex-wall events. The initial reconnections are with vortices toward the longer end of the range, which are more likely to intersect the path of the moving vortex. These events induce Kelvin waves, which make the vortex more likely to encounter the shorter mesh vortices. The short vortices have less direct effect on length, but contribute fully to the Kelvin oscillations along the moving vortex. For a friction coefficient of $\alpha = 0.01$, where the Kelvin oscillations dominate energy loss, a heterogeneous mesh dissipates about 50% more energy than a homogenous mesh with the same mean vortex length. A range of vortex lengths is likely in an experimental setup with irregular wall roughness.

We also consider the orientations of the mesh vortices. Although we generally use entirely random orientations, we also test predominantly horizontal vortices, oriented $\pm 22.5^\circ$ from horizontal in the direction opposite the free vortex precession, and vertical vortices, directed $\pm 45^\circ$ from the upward direction. In each case we take a flat distribution over the selected range of angles. The average dissipation for the random mesh is 30% less than that of the oriented arrangements, as shown in Figure 11. For the horizontal vortices, the length gain from reconnections with the mesh is shorter than for random vortices. Figure 3 illustrates this effect. The red vortex in Figure 3a represents the moving vortex, which is sweeping from right

to left. The black vortex is nearly horizontal and directed in the opposite direction, from left to right. Because of the precession direction and the orientation of the mesh vortices, the vortices meet near the right end of the mesh vortex, and only a short segment of the mesh vortex gets incorporated into the moving vortex. Figure 3d illustrates the situation after the resulting reconnection. The tendency to add mainly short pieces accounts for the overall increase in dissipation for this orientation.

For predominantly vertical vortices, the increase in dissipation arises because the vortex-wall reconnections are particularly effective. The curvature of the cylinder means that vortices with a large vertical component are closer to the wall than those that are mainly horizontal. If a near-vertical mesh vortex is incorporated into the moving vortex, its proximity to the wall facilitates subsequent wall reconnections. The enhanced dissipation from vertical vortices is particularly relevant because in an experimental setup, vortices created during rotation are likely to maintain a predominantly vertical orientation when they partly annihilate at the cell wall after rotation ceases.

Reconnections with pinned vortices have relevance beyond the particular geometry used here, especially in light of the recent interest in turbulence at very low temperatures. In regimes where neither the fluid flow nor temperature can generate vorticity, remnant vortices have long been seen as a source of the new vortex lines needed to sustain turbulence [31]. Other experiments generate turbulence through interactions with solid objects such as oscillating grids or wires. Vortices pinned to these structures may play a role in their large effective mass as they move through superfluid helium [32] as well as directly reducing the onset velocity for turbulence [33]. Recent work on monitoring flow through tracer particles [34] also found that the particles moved much slower than the expected normal fluid velocity, with the discrepancy attributed to vortices pinned to the particles [35] or otherwise distorting their motion [36].

Conclusion

We find that the interaction of a moving vortex with wall mesh vortices increases the energy dissipation rate above that observed without this interaction. At high temperatures the reconnections generate Kelvin waves, which increase the vortex velocity and the resulting dissipation from mutual friction. At lower temperatures the dominant mechanism is that Kelvin oscillations lead to repeated reconnections between the vortex and the wall, which effectively chop off bits of the moving vortex and transfer them to the wall. Our lowest-temperature simulations show the energy loss from the moving vortex increasing by a factor of 100, and the effect could be even larger at the lower temperatures achieved in typical experiments.

We thank A. Smith for running some of the early simulations.

[1] R.J. Donnelly, *Quantized Vortices in Helium II* (Cambridge University Press, Cambridge, England, 1991).

[2] H.E. Hall and W.F. Vinen, "Experiments on the propagation of second sounds in uniformly rotating helium II," *Proc. Roy. Soc.* **A238**, 204-14 (1956); *ibid.*, "The theory of mutual friction in uniformly rotating helium II," *Proc. Roy. Soc.* **A238**, 215-34 (1956).

[3] G.W. Rayfield and F. Reif, "Quantized vortex rings in superfluid helium," *Phys. Rev.* **136**, A1194 (1964).

[4] C.F. Barenghi, R.J.Donnelly, and W.F. Vinen, "Friction on quantized vortices in helium II," *J. Low Temp. Phys.* **52**, 189-247 (1983).

[5] M. Abid et al., "Experimental and numerical investigations of low-temperature superfluid turbulence," *Euro. J. Mech. B, Fluids* **17**, 665 (1998); J. Maurer and P. Tabeling, "Local investigation of superfluid turbulence," *Europhys. Lett.* **43**, 29 (1998).

[6] M.R. Smith, R.J. Donnelly, N. Goldenfeld, and W.F. Vinen, "Decay of vorticity in homogeneous turbulence," *Phys. Rev. Lett.* **71**, 2583 (1993).

[7] P.M. Walmsley et al., "Dissipation of quantum turbulence in the zero temperature limit," *Phys. Rev. Lett.* **99**, 265302 (2007); arXiv:0710.1033.

[8] P.M. Walmsley and A.I. Golov, "Quantum and quasiclassical types of superfluid turbulence," *Phys. Rev. Lett.* **100**, 245301 (2008); arXiv:0802.2444.

[9] M. Tsubota, T. Araki, and S.K. Nemirovskii, "Dynamics of vortex tangle without mutual friction in superfluid ^{4}He," *Phys. Rev. B* **62**, 11751 (2000); arXiv:cond-mat/005280.

[10] D.I. Bradley et al., "Decay of pure quantum turbulence in superfluid 3He-B," *Phys. Rev. Lett.* **96**, 035301 (2006); arXiv:0706.0621.

[11] W.F. Vinen, "Decay of superfluid turbulence at a very low temperature: The radiation of sound from a Kelvin wave on a quantized vortex," *Phys. Rev. B* **64**, 134520 (2001).

[12] D. Charalambous et al., "Quantum turbulence in ^{4}He, oscillating grids, and where do we go next?" *J. Low Temp. Phys.* **145**, 107 (2006).

[13] L.A.K. Donev, L. Hough, and R.J Zieve, "Depinning of a superfluid vortex line by Kelvin waves," *Phys. Rev. B* **64**, 180512(R) (2001); arXiv:cond-mat/0010240 and L. Hough, L.A.K. Donev, and R.J. Zieve, "Smooth vortex precession in superfluid ^{4}He," *Phys. Rev. B* **65**, 024511 (2001); arXiv:cond-mat/0104525.

[14] C.E. Swanson, W.T. Wagner, R.J. Donnelly, and C.F. Barenghi, "Calculation of frequency- and velocity-dependent mutual friction parameters in helium II," *J. Low Temp. Phys.* **66**, 263 (1987).

[15] P.W. Adams, M. Cieplak, and W.I. Glaberson, "Spin-up problem in superfluid ^{4}He," *Phys. Rev. B* **32**, 171 (1985).

[16] C. Frei, D. Wolfson, and R.J. Zieve, to be published.

[17] K.W. Schwarz, "Three-dimensional vortex dynamics in superfluid ^{4}He: Line-line and line-boundary interactions," *Phys. Rev. B* **31**, 5782 (1985).

[18] D.C. Samuels, "Velocity matching and Poiseuille pipe flow of superfluid helium," *Phys. Rev. B* **46**, 11714 (1992).

[19] M. Tsubota and S. Maekawa, "Pinning and depinning of two quantized vortices in superfluid ^{4}He," *Phys. Rev. B* **47**, 12040 (1993).

[20] R.G.K.M. Aarts and A.T.A.M. de Waele, "Numerical investi-

gation of the flow properties of He II," *Phys. Rev. B* **50**, 10069 (1994).
[21] R.G.K.M. Aarts, Ph.D. thesis, Technische Universiteit Eindhoven (1993).
[22] C.F. Barenghi, D.C. Samuels, G.H. Bauer, and R.J. Donnelly, "Superfluid vortex lines in a model of turbulent flow," *Phys. Fluids* **9**, 2631 (1997).
[23] R.J. Zieve and L.A.K. Donev, "Stable vortex configurations in a cylinder," *J. Low Temp. Phys.* **121**, 199 (2000); arXiv:cond-mat/0006078.
[24] From [4]; our α equals $\gamma/\kappa\rho_s$ from that paper.
[25] J. Koplik and H. Levine, "Vortex reconnection in superfluid helium," *Phys. Rev. Let.* **71**, 1375 (1993).
[26] M.S. Paoletti, Michael E. Fisher, K.R. Sreenivasan, and D.P. Lathrop, "Velocity statistics distinguish quantum turbulence from classical turbulence," *Phys. Rev. Lett.* **101**, 154501 (2008); arXiv:0808.1103 and G.P. Bewley, M.S. Paoletti, K.R. Sreenivasan, and D.P. Lathrop, "Characterization of reconnecting vortices in superfluid helium," *Proc. Nat. Acad. Sci*. **105**, 13707 (2008); arXiv:0801.2872.
[27] D.D. Awschalom and K.W. Schwarz, "Observation of a remanent vortex-line density in superfluid helium," *Phys. Rev. Lett*. **52**, 49 (1984).
[28] M. Leadbeater, T. Winiecki, D.C. Samuels, C.F. Barenghi, and C.S. Adams, "Sound emission due to superfluid vortex reconnections," *Phys. Rev. Lett.***86**, 1410 (2001); arXiv: cond-mat/0009060.
[29] D.R. Tilley and J. Tilley, *Superfluidity and Superconductivity* (Institute of Physics Publishing, Bristol, 1990), Chapters 1 and 6, p186, 191-3.
[30] W. Thomson, "Vibrations of a columnar vortex," *Phil. Mag.* **10**, 155 (1880).
[31] R. Hänninen, M. Tsubota, and W.F. Vinen, "Generation of turbulence by oscillating structures in superfluid helium at very low temperatures," *Phys. Rev. B* **75**, 064502 (2007); arXiv:cond-mat/0610224.
[32] D. Charalambous, L. Skrbek, P.C. Hendry, P.V.E. McClintock, and W.F. Vinen, "Experimental investigation of the dynamics of a vibrating grid in superfluid ^{4}He over a range of temperatures and pressures," *Phys. Rev. E* **74**, 036307 (2006).
[33] Y. Nago et al., "Observation of remanent vortices attached to rough boundaries in superfluid ^{4}He," *J. Low Temp. Phys.* **158**, 443 (2010).
[34] T. Zhang and S.W. Van Sciver, "The motion of micron-sized particles in He II counterflow as observed by the PIV technique," *J. Low Temp. Phys.* **138**, 865 (2005).
[35] Y.A. Sergeev, C.F. Barenghi, and D. Kivotides, "Motion of micron-size particles in turbulent helium II," *Phys. Rev. B* **74**, 184506 (2006); **75**, 019904(E) (2007).
[36] D. Kivotides, "Motion of a spherical solid particle in thermal counterflow turbulence," *Phys. Rev. B* **77**, 174508 (2008).